J For Res (2014) 19:329–339
DOI 10.1007/s10310-013-0425-y

ORIGINAL ARTICLE

Dependence of runout distance on the number of rock blocks in large-scale rock-mass failure experiments

Yasuhiko Okada · Ippei Uchida

Received: 25 September 2009 / Accepted: 8 October 2013 / Published online: 23 November 2013

Abstract To examine how the number of rock blocks affects the rock-mass runout distance, large-scale outdoor rockfall experiments were physically performed using cubiform granite rock blocks on a slope prepared with granite slabs under both dry and water-saturated conditions. To learn more about the runout mechanism, numerical simulations were also conducted using three-dimensional DEM to reproduce the physical experiments under dry conditions. Longitudinal rock-mass runout distance between the gravity centre in the initial rock block assembly before failure and the apparent gravity centre at final deposition was 10 % larger for experiments under water-saturated conditions than those under dry conditions, with identical numbers of rock blocks in the physical experiments. The physical and numerical experiments revealed that rock blocks at the front and top surfaces had a longer runout distance than those at the rear and bottom surfaces. A rock block scarcely surpassed the rock blocks in front longitudinally and the rock blocks next to it laterally. The equivalent coefficient of friction between gravity centres was positively correlated with the number of rock blocks, which contradicts the findings of a negative correlation between the volume of sturzstroms (rockfall avalanches) and the equivalent coefficient of friction in classic studies on the long runout mechanisms. Our results were likely attributable to the fact that more kinetic energy was dissipated due to repeated inelastic intercollisions with other surrounding rock blocks and granite slabs when the initial rock-mass volume (number of rock blocks) was larger.

Keywords Equivalent coefficient of friction · Inelastic collision · Number of rock blocks · Rock-mass runout distance

Y. Okada (✉)
Forestry and Forest Products Research Institute, Matsunosato 1, Tsukuba, Ibaraki 305-8687, Japan
e-mail: okada10@ffpri.affrc.go.jp

I. Uchida
Keiyo Gas Company Limited, Ichikawa-minami 2-8-8, Ichikawa, Chiba 272-8580, Japan

Introduction

Landslides are classified into five types: falls, topples, slides, spreads, and flows (Cruden and Varnes 1996). Of these, flows (flow-like landslides) have attracted extended attention because of their longer runout distances. In flows, pore pressure build-up can play a major role, in which soil particles float and the effective stress and shear resistance decline (Hutchinson and Bhandari 1971). To reveal the long runout mechanisms of flow-like landslides, many researchers have conducted various kinds of geotechnical soil tests under both monotonic and cyclic conditions, focusing on the pore pressure build-up (Casagrande 1971; Castro and Poulos 1977; Seed 1979; Poulos 1981; Hutchinson 1986; Ishihara 1993; Sassa 1996), and model slope and flume tests (Iverson and LaHussen 1989; Iverson 1997; Okada and Ochiai 2008). Sturzstroms (rockfall avalanches) are also identified as landslides with longer runout distances (Hsü 1975). Cruden and Varnes (1996) mentioned that sturzstroms are extremely rapid flows of dry debris and their motion probably depends on dispersive stresses arising from momentum transfer between colliding particles. It is also mentioned in Hsü (1975) that a sturzstrom can be defined as a stream of very rapidly moving debris derived from the disintegration of a huge fallen rock mass (lower

limit is 5 million m^3), and sturzstroms do indeed flow. It has been pointed out that the equivalent coefficient of friction of the sturzstroms (rockfall avalanches) was smaller when the volume was larger, and that this relationship was linear on a log–log plot (Scheidegger 1973; Hsü 1975). Furthermore, although the equivalent coefficient of friction is generally estimated with distances measured by taking the front end of the landslides, the gravity centre of the landslide before and after failure has been used by some researchers such as Hsü (1975). Although no plot is shown, Hsü (1975) states that the equivalent coefficient of friction, estimated with the gravity centre of the landslide, is negatively proportional to volume. An 'air-layer lubrication model' (Shreve 1966, 1968) explains some parts of the mechanisms of this relationship, in which larger sturzstroms took in a large volume of air, whereupon the lower friction was mobilised due to increased pore-air pressure.

Many long runout landslides have been observed in Japan, and even though the number has declined somewhat in recent years, they still occur almost every year. Typical examples include the 1999 Kameyama debris flow in Hiroshima Prefecture, the 2003 Minamata debris flow in Kumamoto Prefecture, the 2005 Wanizukayama debris flow in Miyazaki Prefecture, and the 2008 Shimizuyama rock flow in Miyagi Prefecture. Although the first four examples were induced by rainfall, the last one was caused by an earthquake. Because the volume of the Shimizuyama rock flow was only in the order of 10^5 m^3, it would not be called a sturzstrom. In the case of Shimizuyama, the travel distance far exceeded that expected from its relatively small volume and promoted further study of the mechanisms of its motion. Prompted by the Kameyama debris flow, a new law was enacted emphasising the importance of risk management, preparation and publication of landslide hazard maps by local governments. Urgent efforts were required by researchers to facilitate understanding of the mechanism of longer runout distances and establish an optimum system to mitigate such landslides.

Regarding long runout flow-like landslides, the distinct element method (DEM) (Cundall and Strack 1979) has been applied to reproduce longer runout distances. Kiyama and Fujimura (1983) numerically simulated the gravity flow of rock-like granular materials by 2-dimensional (2D) DEM, whereas Tarumi and Hakuno (1987) applied 2D DEM to rockfall avalanches and debris flows to clarify the mechanism of large rocks floating up to the flow surface and their subsequent aggregation at the front of the surge. However, the DEM poses some difficulties in fine-tuning the parameters and is rather time-consuming when numerous numerical balls (in 3D) or discs (in 2D) are used. Hakuno (1997), however, cited the advantage of the method for simulating phenomena such as rock-mass failure, involving detachment, collision, and sliding of rock blocks. Challenges to fluid-coupling in DEM have also been undertaken: Kiyama et al. (1994) and Tarumi and Hakuno (1987) investigated the generation of excessive pore-water pressure under undrained conditions in two dimensions, while Ng and Dobry (1994) employed 3D DEM to investigate the reduction of effective normal stress under constant volume conditions; and Okada and Ochiai (2007) and Okada (2011) conducted undrained triaxial compression tests and examined the relationship between the effective angle of internal friction and the void ratio. Hakuno and Tarumi (1988) pointed out the need to use 3D DEM to study pore pressure build-up, since the mechanisms cannot be modelled in two dimensions.

Although many studies have been reported on the long runout mechanism using DEM, the number of numerical balls used was generally limited and it was not possible to reproduce the movement of individual fine particles. Therefore, the numerical balls or discs modelled the aggregation of several fine particles (Okada and Ochiai 2007). Regarding the rockfall experiments, Okura et al. (2000) performed physical rockfall experiments and a DEM simulation with equivalent numbers of rock blocks and numerical balls. In their study, a prop was withdrawn to initiate the rock fall after adjusting the container inclination to horizontal on the experimental slope. The initial velocities of the blocks in this procedure differed in each case, while the method used to trigger the rock fall also differed between the simulation and experiment. In addition, the physical experiments were only conducted under dry conditions and the effect of water, which would affect the runout distance, was not taken into consideration.

In this study, to reveal the downslope behaviour of rockfall and clarify the relationship between rock-mass runout distance and number of rock blocks, large-scale physical rockfall experiments using cubic assemblies of granite rock blocks were performed. The size of the blocks was approximately 0.1 m^3 and the maximum number of blocks used in the experiment was 1,000. The experiments were conducted under dry and water-saturated conditions, while 3D DEM simulations were performed under dry conditions.

Rockfall experiment

Rockfall apparatus and experimental slope

Figure 1 shows the rockfall apparatus and experimental slope, while Fig. 2 illustrates the schematics of the longitudinal section of the rockfall apparatus. Although it is important to satisfy the scaling conditions for a physical phenomenon dominated by the expression of force and

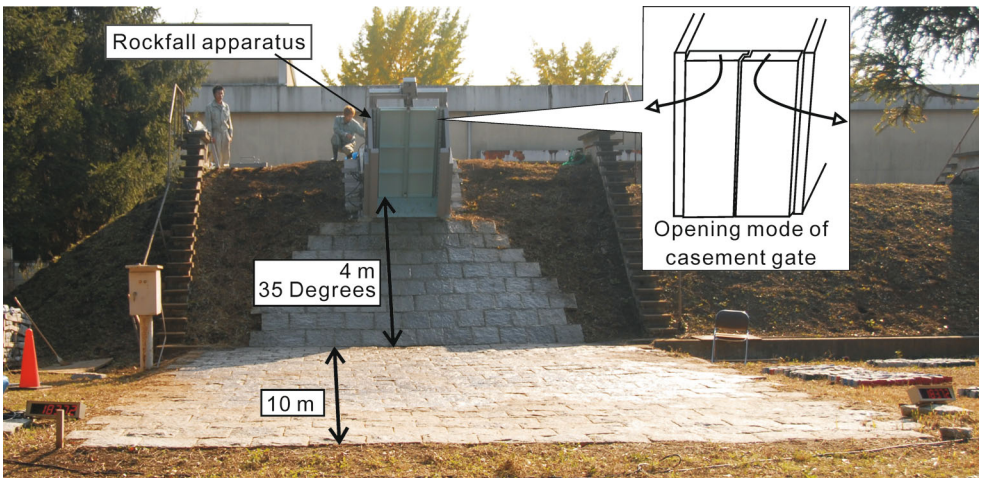

Fig. 1 Large-scale rockfall apparatus and experimental slope

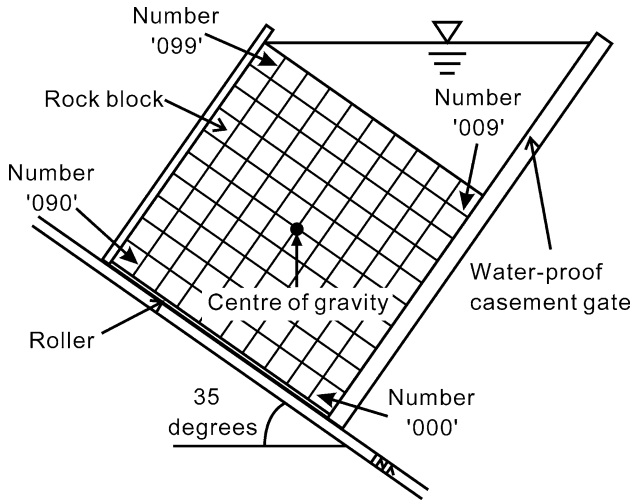

Fig. 2 Schematic section of rockfall apparatus

stress, such as rock-mass failure and granular mass flow (Kagawa 1978; Iverson 1997), past studies have mostly used small-scale models lacking correct scaling. In this study, rock-mass failure experiments were conducted using a large-scale rockfall apparatus. To facilitate these experiments, this apparatus was developed capable of holding 1,000 cubiform rock blocks, where each block was 0.1 m^3 and the total volume of the cubic assembly was 1 m^3. The rockfall apparatus is made from stainless steel, with rollers (thin stainless steel pipes 0.015 m in diameter, 1 m long) situated longitudinally every 0.05 m on the bottom surface, enabling rock blocks to slide down easily when the sliding was triggered. Since commercially available cubiform rock blocks were used, a cubiform-shaped rock block assembly was formed in the rockfall apparatus, for the sake of efficiency in specimen preparation and ease of shape similarity in each experiment. In addition, to perform experiments with the rock block assembly under water-saturated conditions, the casement gate was processed for water-proofing. The opening of the casement gate was also electronically controlled to release the rock blocks at the start of each experiment, while stainless steel interior tanks were installed to maintain a consistent volume ratio of water to rock blocks for experiments under water-saturated conditions.

The slope, consisting of inclined and horizontal sections, was prepared with granite slabs (0.4 m long, 0.4 m wide, 0.06 m thick) and the inclination was set at 35°, enabling rock blocks to slide down the slope by their own weight just after the gate opened. This inclination was the same as that of the large-scale flume apparatus for granular mass flow experiments (Okada and Ochiai 2008). The length of the inclined portion of the slope was set at 4 m, which is equivalent to that of the flume apparatus. The inclination and slope length were kept constant throughout the experiments in this study due to difficulties in changing the experimental setup, while the effects of these parameters will be covered in future work. The width of the inclined section of the slope was 2 m at the gate location and made wider towards the location where the inclined portion connects with the horizontal section (Fig. 1). The width was about 6 m in the horizontal section, which extended longitudinally to 10 m allowing rock-mass deposition over a wide area.

Rock block assembly and experimental conditions

The rock blocks used were of granite and cubiform (c. 0.1 m^3), and a maximum of 1,000 blocks were placed in the rockfall apparatus for an experiment. Each rock block was sequentially numbered and specifically arranged in the rockfall apparatus to allow us to identify its initial position. In detail, the rock block was numbered by three digits, from '000' to '999' from smallest to largest. For example, the rock block number '000' was set at the far right

position, furthest downslope, and on the bottom surface. The numbers '000,' '090,' '009,' and '099' are also shown in Fig. 2 as examples. Medium-speed (60 frames/s) and low-speed (30 frames/s) digital video cameras were configured as stereo pairs to film the rock-mass downslope motion during the experiments. Digital timers, with a resolution of 0.01 s, were attached to the experimental slope to film the elapsed time together with the falling blocks. Using this system, the films were almost synchronised. When rock blocks were deposited, the longitudinal runout distance was measured for each rock block as fundamental data for examining rock-mass downslope movements.

Regarding the rock-mass runout behaviour, it was found that the density of rock blocks, kinetic friction, and coefficient of restitution were among the most important parameters, as were the inclination, length, and shape of the experimental slope section. The density of rock blocks was calculated by measuring the dry weight and the equivalent volume was replaced by distilled water. Kinetic friction was calculated by measuring the traction force of a granite rock block over the granite slab (Fig. 3a), while the coefficient of restitution was estimated using two methods. Firstly, one block was made to hit another, initially in a stationary position as shown in Fig. 3b. Secondly, a block was made to hit a granite slab as shown in Fig. 3b. The speeds of the blocks before and after collisions were measured by image analysis. The images were filmed by medium-speed digital video cameras and the average coefficient of restitution was 0.37 between two rock blocks, and 0.40 between a rock block and a slab. Mizuyama (1979) showed a coefficient of restitution between concrete and rock blocks of about 0.4, which resembles the results obtained by the tests described here. Measurements were conducted using four rock blocks, and, particularly for kinetic friction and coefficient of restitution, were repeated at least five times per rock block to obtain averaged values.

In addition to kinetic friction, a rolling friction, which was introduced by Okura et al. (2000), may need to be taken into consideration. Okura et al. (2000) estimated the rolling friction by determining the inclination at which the blocks rolled down at uniform speed without sliding. Although no figures or detailed explanations were found in the paper by Okura et al. (2000), a very large-scale slope section with variable inclination would be required for the 0.1-m^3 rock blocks to roll down the slope at uniform speed. However, this would be quite difficult. In addition, rolling

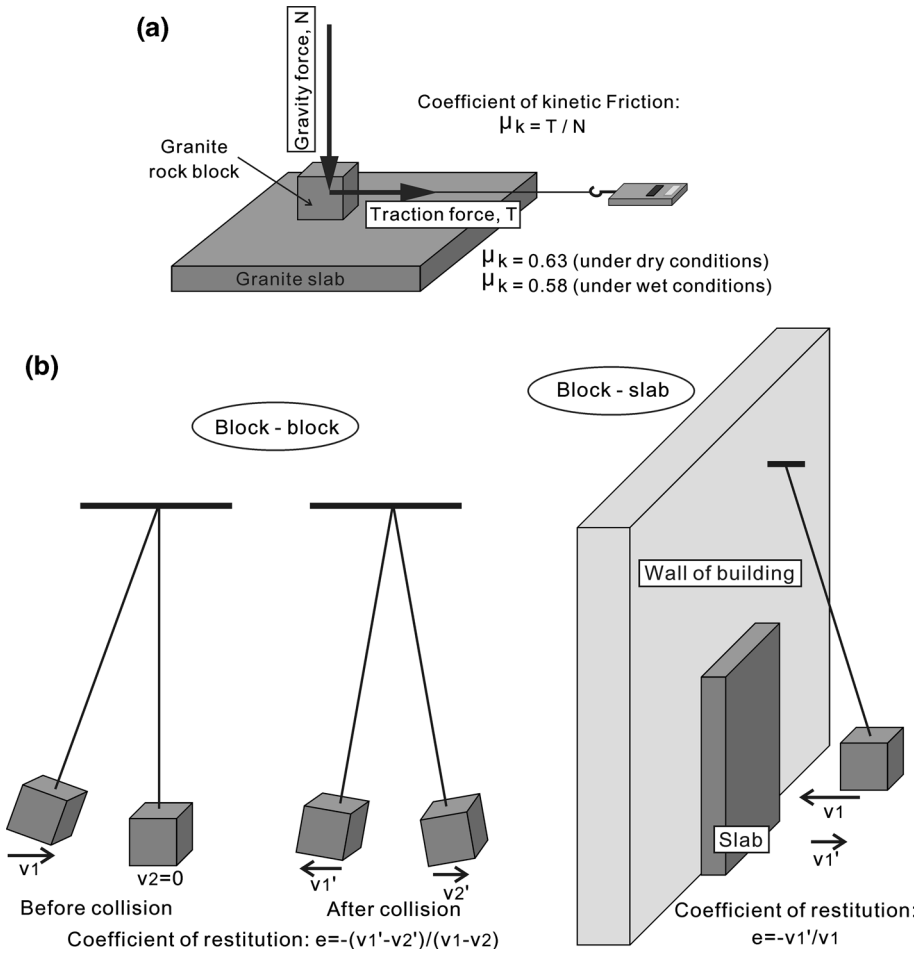

Fig. 3 Schematic illustration of fundamental experiment on sliding and collision of rock blocks. **a** Coefficient of kinetic friction, **b** coefficient of restitution

Table 1 Identification number and conditions of physical experiments

Experiment no.	Number of blocks	Volume (m^3)	Dry/saturated
Ex-D1	27 (3 × 3 × 3)	0.0270	Dry
Ex-D2	125 (5 × 5 × 5)	0.125	Dry
Ex-D2'	125 (5 × 5 × 5)	0.125	Dry
Ex-D3	343 (7 × 7 × 7)	0.343	Dry
Ex-D4	1,000 (10 × 10 × 10)	1.00	Dry
Ex-S1	27 (3 × 3 × 3)	0.0270	Saturated
Ex-S2	125 (5 × 5 × 5)	0.125	Saturated
Ex-S3	343 (7 × 7 × 7)	0.343	Saturated
Ex-S4	1,000 (10 × 10 × 10)	1.00	Saturated

Table 2 Parameters of rock blocks

Parameters of rock blocks		
Coefficient of kinetic friction	0.63 (dry)	0.58 (wet)
Coefficient of restitution	0.37 (block–block)	0.40 (block–slab)
Density	2,540 kg m^{-3}	

friction is usually introduced when analysing rolling resistance caused by the deformation of round-shaped objects, such as tyres, when subjected to compressive force. However, rolling friction was not measured in this research, since the blocks were cubic in shape, making it difficult to determine.

Physical experiments were conducted under dry and water-saturated conditions, with the experiment identification number and conditions shown in Tables 1 and 2. The water table in the water-saturated experiments was at the highest position for the arranged rock blocks, indicating a greater water depth in zones closer to the gate in the rockfall apparatus (Fig. 2). As mentioned above, interior tanks were installed for water-saturated experiments to maintain a consistent volume ratio of water volume to rock blocks. The measurement in Ex-S3 showed a ratio of water volume to rock blocks of about 6:5. The same rock blocks were repeatedly used in the experiments and showed little sign of frictional wear, particularly on the edges. Accordingly, after all the experiments had been conducted, an additional experiment (Ex-D2′) was conducted under the same conditions as in Ex-D2.

Numerical simulation

To learn more about the rock-mass runout behaviour mechanism, the numerical simulation of the rockfall experiment was conducted by 3D DEM (distinct element method). The numerical block was modelled with eight rigidly connected ball elements, in which the centre of a ball element was positioned 0.02 m from the centre of a neighbouring ball element (Fig. 4). Note that, since it is too complicated to show all eight balls, only three balls and the centres of eight balls are presented in Fig. 4. The radius of the ball elements was randomly modified between 0.025 and 0.055 m with an average of 0.040 m, since the rock block was not a perfect cube and had an irregular surface. Each model block was numbered to match the numbers assigned to the block used in the experiments so that the initial position could be traced.

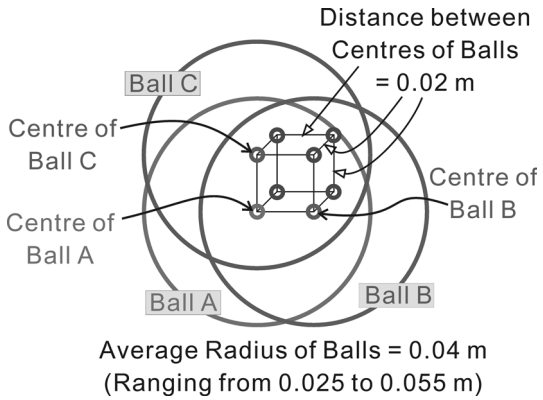

Fig. 4 Schematic illustration of a numerical rock-block element consisting of eight ball elements (note that only three ball elements are depicted to avoid confusion)

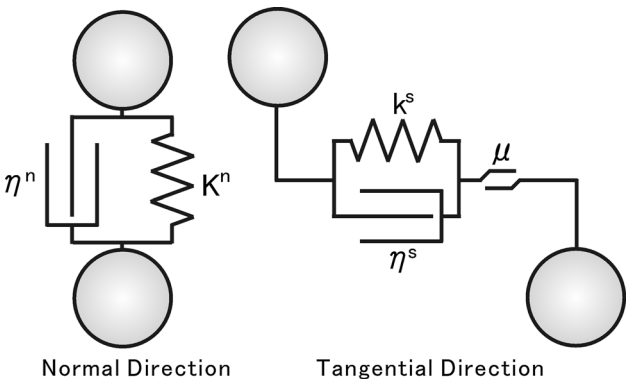

Fig. 5 Force transmission system in ball–ball contact in normal, tangential, and rotational directions

In DEM, the force transmission between two ball elements was modelled with elastic springs, viscous dashpots, and sliders in normal and tangential directions (Fig. 5). In the 1-dimensional mass-spring-dashpot system, the equation of motion of a ball in the translational direction is governed by Eq. 1 (Cundall and Strack 1979; Kiyama and Fujimura 1983).

$$m\ddot{x} + \eta^n \dot{x} + k^n x = 0 \quad (1)$$

where m is the mass of the ball element, K^n is the elastic spring stiffness, η^n is the viscous damping coefficient and $\ddot{x}$ and $\dot{x}$ are acceleration and velocity. Regarding the value of

K^n, Kiyama and Fujimura (1983), Uchida and Hakuno (1988), and Hakuno and Tarumi (1988) determined the elastic spring stiffness in the normal direction by a contact theory for an elastic cylinder. In addition, the elastic spring stiffness in the tangential direction (k^s) was given by the ratio of shear modulus (G) to Young's modulus. Hakuno (1997) states that elastic spring stiffness in the normal direction should be taken as a tuning parameter and was estimated by trial and error, since elastic spring stiffness is not the same as Young's modulus. In this study, the elastic spring stiffnesses in normal and tangential directions were set at $9.0 \times 10^{3.0}$ and $2.5 \times 10^{1.0}$ N m^{-1}, so that the experimental results could be reproduced and in order to keep the computational speed reasonable. The viscous damping coefficient in the normal direction was related to the coefficient of restitution (Ohmachi and Arai 1986).

$$\eta^n = 2h_n\sqrt{mK^n} \tag{2}$$

$$h_n = \sqrt{(\ln e)^2 \Big/ \left(\pi^2 + (\ln e)^2\right)} \tag{3}$$

where h_n is an attenuation constant and e the coefficient of restitution. As the coefficient of restitution of the granite rock blocks was about 0.37, the calculated attenuation constant was 0.30. The viscous damping coefficient in the tangential direction was obtained by

$$\eta^s = \sqrt{s} \times \eta^n \tag{4}$$

$$s = k^s/K^n \tag{5}$$

where s is the taper rate (Kiyama and Fujimura 1983). The critical time-step (Δt) is $\Delta t = \sqrt{\frac{m}{K^n}}$. The particle friction coefficient was set at 0.63 (corresponding to a friction angle of 32°), which was determined based on the coefficient of kinetic friction between a granite rock block and slab under dry conditions. The identification number, conditions, and input parameters are given in Table 3.

The equation of motion of a rock block element is described in terms of translational (Eq. 6) and rotational motion (Eq. 7) (Ginsberg 1995).

$$[F_i]_t = \sum_{b=1}^{Nb}\left[F_i^b\right]_t = \sum_{b=1}^{Nb}\left\{\sum_{c=1}^{Nc}\left(\left[E_i^b\right]_t + \left[D_i^b\right]_t\right) + m_b[g_i]\right\} = m_c\left[\ddot{x}_i^G\right]_t \quad (i = 1, 2, 3) \tag{6}$$

$$[M_i]_t = \sum_{b=1}^{Nb}\left[\varepsilon_{ijk}\left(\left[x_j^b\right]_t - \left[x_j^G\right]_t\right)\left[F_k^b\right] + \sum_{c=1}^{Nc}\left\{\varepsilon_{ijk}\left(\left[x_j^c\right]_t - \left[x_j^b\right]_t\right)\left(\left[E_k^b\right]_t + \left[D_k^b\right]_t\right)\right\}\right] = I[\dot{\omega}_i]_t \quad (i,j,k = 1, 2, 3) \tag{7}$$

where N_b is the number of ball elements consisting of a numerical rock block, N_c is the number of contacts in a ball element, $[E_i^b]$ is the elastic spring force acting on a ball element, $[D_i^b]$ is the viscous damping force acting on a ball element, m_b is the mass of the ball element, m_c is the mass of the numerical block, $[x_i^G]$ is the central position of a rock block element, $[x_i^b]$ is the centre of a ball element, $[x_i^c]$ is the contact point of a ball element, and $[g_i]$ is the gravitational acceleration. The detailed calculation procedures for $[E_i^b]$ and $[D_i^b]$ are shown in Okada and Ochiai (2007). By integrating these equations, the velocity, position, angular velocity, and rotation angle are calculated as:

$$[\dot{x}_i]_{t+\Delta t/2} = [\dot{x}_i]_{t-\Delta t/2} + [\ddot{x}_i]_t \times \Delta t \quad (i = 1, 2, 3) \tag{8}$$

$$[x_i]_{t+\Delta t} = [x_i]_t + [\dot{x}_i]_{t+\Delta t/2} \times \Delta t \quad (i = 1, 2, 3) \tag{9}$$

$$[\omega_i]_{t+\Delta t/2} = [\omega_i]_{t-\Delta t/2} + [\dot{\omega}_i]_t \times \Delta t \quad (i = 1, 2, 3) \tag{10}$$

$$[\theta_i]_{t+\Delta t} = [\theta_i]_t + [\omega_i]_{t+\Delta t/2} \times \Delta t \quad (i = 1, 2, 3) \tag{11}$$

By using position ($[x_i]_{t+\Delta t}$), velocity ($[\dot{x}_i]_{t+\Delta t/2}$), rotation angle ($[\theta_i]_{t+\Delta t}$), and angular velocity ($[\omega_i]_{t+\Delta t/2}$), the values at the next time-step are calculated by repeating the procedures mentioned above.

Table 3 Identification number and input parameters for numerical experiments

Identification number	Number of blocks	Volume (m^3)
Ex-N1	27 (3 × 3 × 3)	0.0270
Ex-N2	125 (5 × 5 × 5)	0.125
Ex-N3	343 (7 × 7 × 7)	0.343
Ex-N4	1,000 (10 × 10 × 10)	1.00
Input parameter		
Normal elastic spring stiffness, K^n	$9.0 \times 10^{3.0}$ N m^{-1}	
Tangential elastic spring stiffness, k^s	$2.5 \times 10^{1.0}$ N m^{-1}	
Normal viscous damping stiffness, η^n	$2.9 \times 10^{3.0}$ Ns m^{-1}	
Tangential viscous damping stiffness, η^s	$1.5 \times 10^{2.0}$ Ns m^{-1}	
Coefficient kinetic friction	0.63	
Coefficient of restitution	0.37	
Density	2,540 kg m^{-3}	

Results

Figure 6 shows an example of the views of rock-mass downslope motion (Ex-S3), (a) 0.25 s, (b) 1.0 s, (c) 2.0 s, and (d) 3.5 s after the gate was opened. Rock blocks and water came out the instant the casement gate opened (Fig. 6a). A front rock block reached the transition point of inclined to horizontal sections at 1 s, but some rock blocks still remained in the rockfall apparatus. A water front was

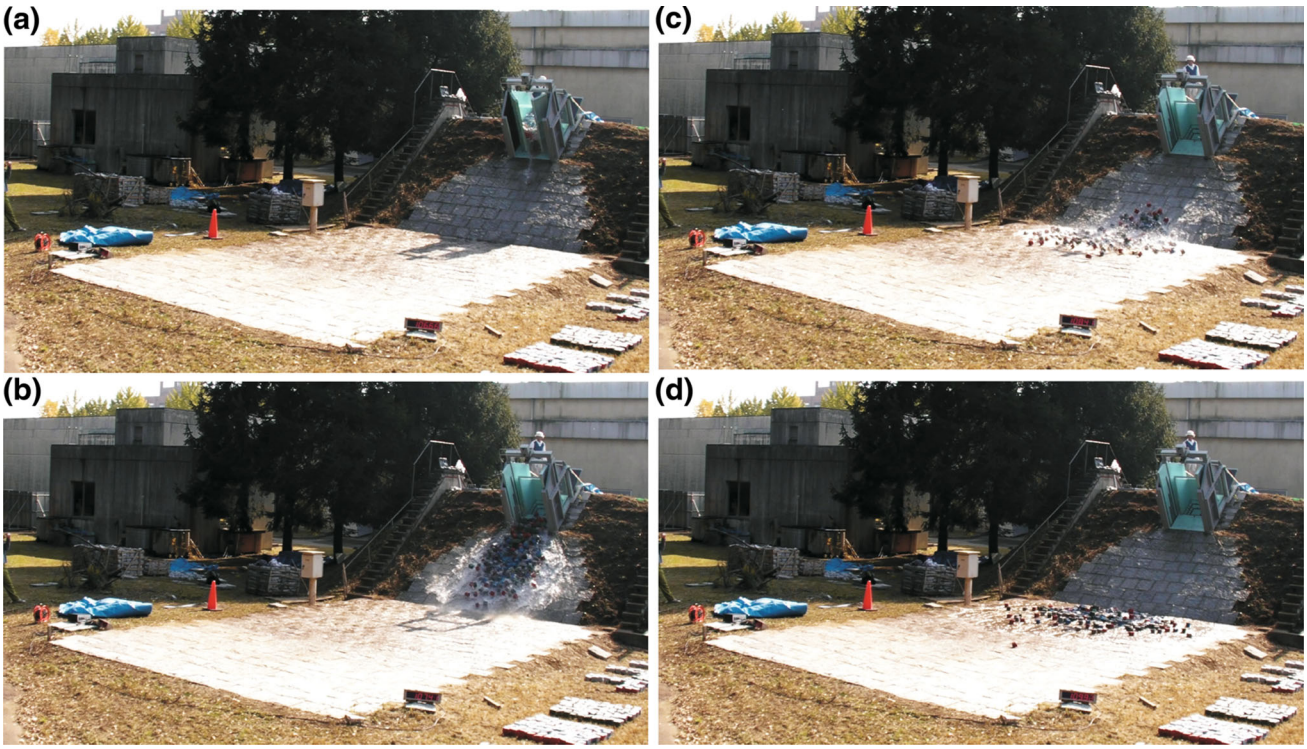

Fig. 6 Example of views of rock-mass failure in Ex-S3 between 0.25 and 3.5 s after the gate opens. **a** 0.25 s, **b** 1 s, **c** 2 s, and **d** 3.5 s

formed about 0.3 m ahead of the rock blocks and the water spread wider than the falling rock blocks by 0.5 m on both sides (Fig. 6b). Most of the rock blocks reached the horizontal part and water splashing was observed at 2.0 s (Fig. 6c), while at 3.5 s, all rock blocks had been deposited (Fig. 6d). The nominal depth of falling rock blocks was relatively shallow, in the order of three or four times the block size, because some of the blocks remained in the container and the blocks spread out while travelling down.

On the longitudinal runout distance

The longitudinal runout distance of rock-mass failure is examined, in which an apparent centre of gravity of the block assembly will be defined as the averaged coordinates of the centre of gravity of all the blocks (a schematic of measurement of the runout distance is shown in Fig. 7). The moving distance of the nominal centre of gravity of the blocks is used rather than the maximum runout distance in analysing the travel distance in terms of potential and kinetic energies (Okura et al. 2000; Okada and Ochiai 2008). Therefore, the longitudinal runout distance of rock-mass failure was measured between the gravity centre of the rock block assembly before failure and the gravity centre at deposition (Fig. 8). A clear relationship between the number of rock blocks and the longitudinal runout distance between gravity centres was found in physical experiments under both dry and water-saturated conditions. The larger the number of rock blocks, the smaller the longitudinal runout distance between gravity centres. When plotting the cube root of the number of rock blocks with respect to the number of blocks, this is linear (Fig. 8). The longitudinal runout distance between gravity centres in numerical experiments was also negatively proportional to the number of numerical rock blocks.

It was also found that the longitudinal runout distance between gravity centres in the experiments under water-saturated conditions was about 10 % larger than that in experiments under dry conditions when the number of rock blocks was the same, which is likely attributable to the following:

1) Kinetic friction between rock blocks, and rock block and granite slab under wet conditions was less than that under dry conditions (Table 2);
2) Rock blocks surrounded by water reduced their effective weight due to buoyancy during the initial sliding process; and
3) Water drag was exerted during the downslope movement.

The longitudinal runout distance between gravity centres in the last experiment (Ex-D2′) was 0.10 m larger than that in Ex-D2 under the same conditions, which could be due to the effect of frictional wear. However, since this had

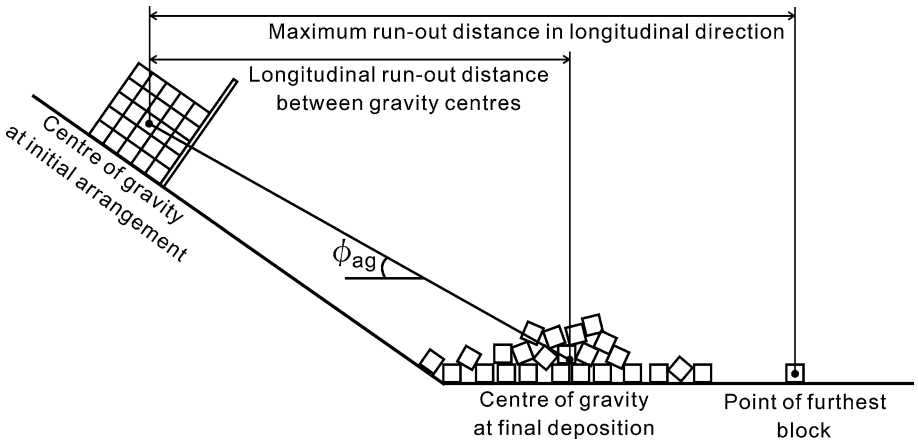

Fig. 7 Conceptual scheme for the longitudinal runout distance between gravity centres

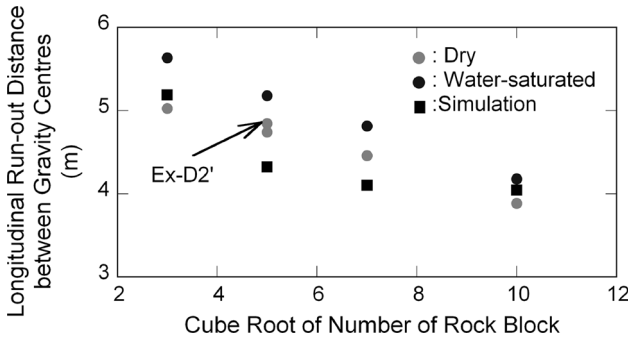

Fig. 8 Relationship between the longitudinal runout distance between gravity centres and the number of rock blocks

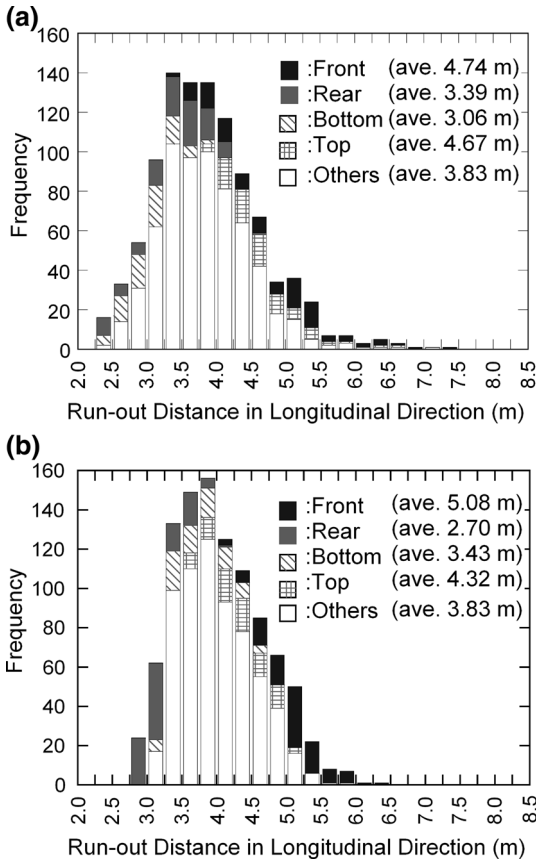

Fig. 9 The runout distance in a longitudinal direction and the frequency of rock blocks at the front, rear, bottom, and top surfaces. **a** Ex-D4, **b** Ex-N4

little effect when evaluating the longitudinal runout distance between gravity centres from a qualitative perspective (Fig. 8), the effect of frictional wear on the runout distance was excluded in this study.

Positions of rock blocks in the assembly before failure and at final deposition

Since the rock block assembly was prepared as a cubiform, it has six surfaces. Here, the runout distances of individual rock blocks located at the front, rear, top, and bottom surfaces in the initial arrangement are analysed. Figure 9a shows a histogram and the frequency of rock blocks in Ex-D4. It is obvious that the rock blocks located at the front and top surfaces had longer longitudinal runout distances and those at the rear and bottom surfaces had shorter distances. The longitudinal runout distance was calculated by averaging the distances measured from the gravity centre of the rock block assembly before failure, which were 4.74 m at the rock blocks at the front surface, 4.67 m at the top surface, 3.39 m at the rear surface, and 3.06 m at the bottom surface, respectively. The results of Ex-N4 are shown in Fig. 9b, where it is again obvious that the rock blocks at the front and top surfaces travelled a longer distance, and those at the rear and bottom surfaces travelled less. The averaged longitudinal runout distance was 5.08 m at the front surface, 4.32 m at the top surface, 2.70 m at the rear surface, and 3.43 m at the bottom surface, respectively. Although the histogram data shown here cover only Ex-D4 and Ex-N4, the longer runout distance for rock blocks at the front and top surfaces was observed in all experiments.

Film images recorded by digital video cameras revealed that the rock blocks located at the front surface were

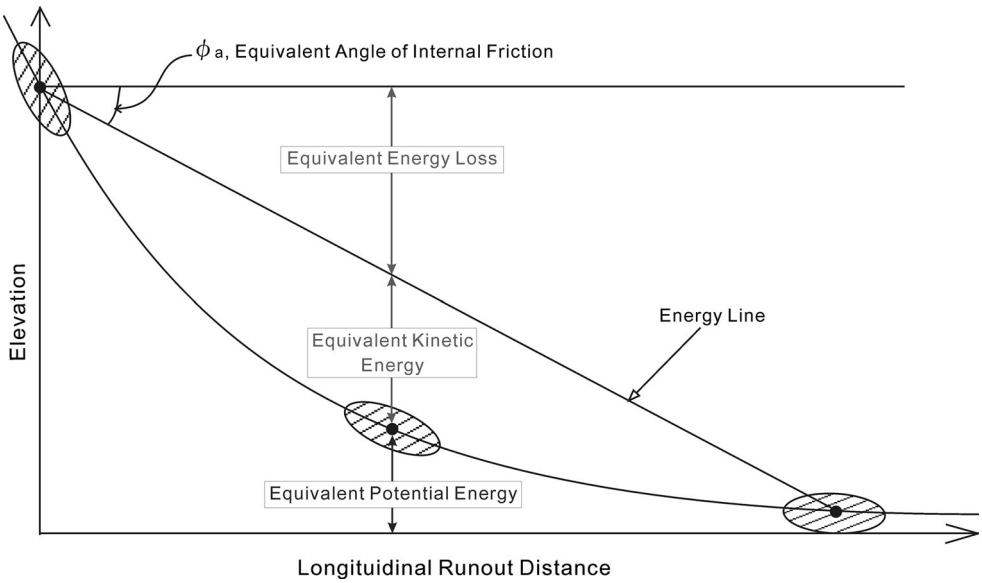

Fig. 10 Conceptual illustration of the energy line

scarcely surpassed by the rock blocks behind and were propelled due to intercollisions between the rock blocks behind. However, the rock blocks at the rear surface hardly surpassed those in front and their movement tended to decelerate due to the intercollision of rock blocks in front. These were the same for the lateral directions, while the rock blocks inside scarcely surpassed the rock blocks outside in the transverse direction. Rock blocks at the top surface had the second-longest longitudinal runout distance after the front-surfaced rock blocks, most likely because (1) top-surfaced rock blocks had relatively higher potential energy before failure, and (2) collisions with other rock blocks mostly occurred at their bottom surfaces with less restriction of movement in the upper direction. Conversely, rock blocks at the bottom surface showed a smaller longitudinal runout distance likely due to the following:

1) Relatively low potential energy before failure;
2) Energy loss due to friction and inelastic collisions during downslope motion;
3) Restriction against free movements due to the surrounding rock blocks.

Discussion

As mentioned above, the equivalent coefficient of friction estimated with the distances measured taking the front end and the equivalent coefficient of friction between the gravity centre before failure and that at deposition was also negatively proportional to the volume of sturzstroms (rockfall avalanches). In the analysis of equivalent coefficient of friction, the energy conversion during downslope movement is generally discussed in terms of the energy line (Fig. 10; note that the x-axis is for the longitudinal distance between gravity centres of the rock-mass). Before landslide initiation, the line has potential energy. During downslope movement, some of the potential energy is converted to kinetic energy and some is lost due to friction, inelastic collisions, etc. The potential, translational kinetic, and rotational kinetic energies are as follows:

$$T_p = \sum_{N_r} m_c g Z \tag{12}$$

$$T_t = \sum_{N_r} \frac{1}{2} m_c [V_i]_c \cdot [V_i]_c \quad (i = 1, 2, 3) \tag{13}$$

$$T_r = \sum_{N_r} \left\{ \frac{1}{2} [\omega_i]_c^T [I_{ij}]_c [\omega_j]_c \right\} \quad (i,j = 1, 2, 3) \tag{14}$$

where N_r is the number of numerical rock blocks, Z is elevation, $[V_i]_c$ is velocity vector, $[\omega_i]_c$ is angular velocity vector, and $[I_{ij}]_c$ is inertia tensor. In Fig. 10, each energy mode is divided by the summation of inertia weight ($\sum_{N_r} m_c g$) for expressions in dimensions of elevation, and they are referred to as equivalent potential energy and equivalent kinetic energy in this study. The larger the inclination of the energy line, the more energy is lost during downslope movement. Figure 11a shows the energy line for the numerical rockfall experiments, the incline of which clearly steepens in numerical experiments with numerous blocks. Since the potential energy is controlled by geomorphological conditions (slope shape), the kinetic energy (translational plus rotational energy) was calculated (Fig. 11b). The kinetic energy was smaller in numerical experiments with more blocks, indicating that less potential

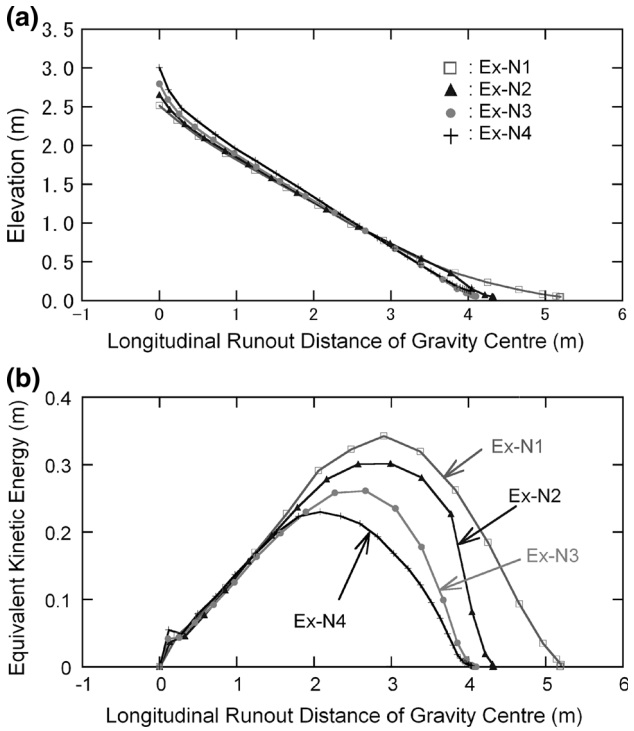

Fig. 11 Relationship of equivalent energy versus longitudinal runout distance of gravity centre. **a** Energy line, **b** kinetic energy

energy was converted to kinetic energy in such experiments. It is noted that gravity centres of rock block assembly formed in the rockfall apparatus differed between experiments due to differing numbers of blocks. Although the potential energy at the initial arrangement was larger in numerical experiments with more blocks, the converted kinetic energy was smaller. Equivalent coefficients of friction between the gravity centre of the rock block assembly before failure and the gravity centre at deposition in all physical and numerical experiments are shown in Fig. 12. It is also shown that the equivalent coefficient of friction between gravity centres was larger when the initial volume of rock block assembly was larger. This contradicts findings in classic studies which showed a negative correlation between the equivalent coefficient of friction and the volume of the sturzstrom (rockfall avalanche). Note that the equivalent coefficient of friction of Ex-N2 and Ex-N3 showed larger values than Ex-P2 and Ex-P3, while Ex-N4 showed the smaller equivalent coefficient of friction than Ex-P4. This is likely attributable to the facts that the rock block in the physical experiment was cubiform with rough and uneven surfaces, but the numerical rock block was modelled by rigidly connecting ball elements. Accordingly, a numerical simulation could not necessarily reproduce all the complicated runout behaviour of the rock blocks in the physical experiment.

Since the nominal depth of rock-mass failure was found to be about three or four times the size of blocks when the

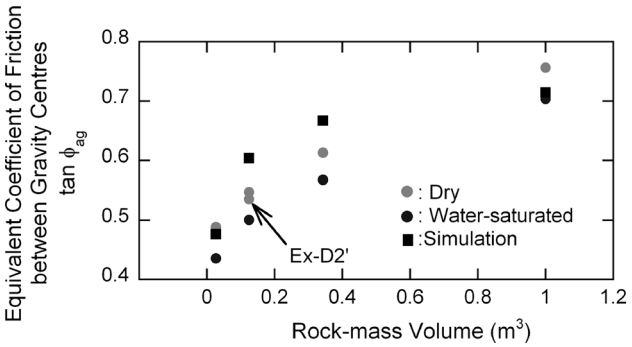

Fig. 12 Equivalent coefficient of friction between gravity centres in positive correlation with rock-mass volume (number of rock blocks)

rock-mass moved down the slope (see Fig. 6), it appeared that pore structures were not formed in the rock-mass. Due to rapid water pressure dissipation, even in the rock-mass under water-saturated conditions, there were no significant differences in travel distances from the experiments under dry conditions. A rock block moves down the slope, repeatedly colliding with other rock blocks or slab surfaces. When a rock block is surrounded by other rock blocks, repeated intercollisions take place longitudinally as well as laterally and also in the up-and-down directions. Neighbouring rock blocks prevented the rock block from rotating to travel further down the slope. Since the coefficient of restitution between two rock blocks was about 0.37, kinetic energy was consumed every time rock blocks collided during the downslope movement. Film images revealed that rock blocks in experiments with few rock blocks moved down the slope separately with few inelastic intercollisions, whereas those in experiments with numerous rock blocks were surrounded by other blocks. The equivalent coefficient of friction between gravity centres before and after failure is positively proportional to the total volume of the rock block assembly due to energy loss, which tends to be larger when there are more blocks.

Concluding remarks

Physical and numerical rock-mass failure experiments were performed with a maximum rock-mass volume of 1 m^3. This maximum volume meant dynamic movements of rock-mass may not necessarily represent those of actual rockfalls. However, in evaluating the mechanism of the downslope movement of granular materials, some interesting findings were drawn from rockfall experiments using the cubiform rock block assembly falling on a slope 4 m long with an inclination of 35°.

- In the physical experiments with an equivalent number of rock blocks, the longitudinal runout distance was

about 10 % longer for the rock block assembly under water-saturated conditions compared to that under dry conditions. This was likely attributable to the fact that: (1) kinetic friction between rock blocks, and rock blocks and granite slabs was smaller under wet conditions; (2) the effective weight of rock blocks was smaller due to buoyancy force; and (3) water drag was exerted.

- The final location of a block was found to be related to the initial location of the block among the cubiform rock block assembly before failure: the rock blocks at the front and top surfaces of the initial assembly had a longer longitudinal runout distance, whereas the rock blocks at the rear and bottom surfaces of the initial assembly had a shorter longitudinal runout distance.
- The equivalent coefficient of friction between the gravity centre of the initial rock block assembly before failure and the averaged coordinates of the centre of gravity of all rock blocks at deposition was proportional to the initial rock-mass volume (number of rock blocks) in our experiments. This was likely because more kinetic energy dissipated due to repeated inelastic intercollisions with surrounding other rock blocks and granite slabs when the initial rock-mass volume (number of rock blocks) was larger.

Acknowledgments We thank Mr. Hiroyuki Miyajima (Yokoyama Rubber Co., Ltd.) for his immense help in preparing rock block assemblies and measuring the distance of each rock block in the experiments with 1,000 rock blocks. We also thank Drs. Hirotaka Ochiai, Toshiaki Sammori (Forestry and Forest Products Research Institute), and Prof. Sumio Matsuura (Disaster Prevention Research Institute, Kyoto University) for their valuable suggestions and advice on the analysis of rock block runout behaviour.

References

Casagrande A (1971) On liquefaction phenomena. Géotechnique 21(3):197–202

Castro G, Poulos SJ (1977) Factors affecting liquefaction and cyclic mobility. ASCE J Geotech Eng Div 103(GT6):501–516

Cruden DM, Varnes DF (1996) Landslides, investigation and mitigation: special report 247. In: Turner AK, Schuster RL (eds) Landslide types and processes. Transportation Research Board, National Research Council, Washington, DC, pp 36–75

Cundall PA, Strack ODL (1979) A discrete numerical model for granular assemblies. Géotechnique 29:47–65

Ginsberg JH (1995) Advanced engineering dynamics, 2nd edn. Cambridge University Press, New York

Hakuno M (1997) Numerical simulation for failures. Morikita, Tokyo (in Japanese)

Hakuno M, Tarumi Y (1988) A granular assembly simulation for the seismic liquefaction of sand. Proc Jpn Soc Civil Eng 398(I–10):129–138

Hsü KJ (1975) Catastrophic debris streams, sturzstroms generated by rockfalls. Geol Soc Am Bull 86:129–140

Hutchinson JN (1986) A sliding-consolidation model for flow slides. Can Geotech J 32:610–623

Hutchinson JN, Bhandari RK (1971) Undrained loading, a fundamental mechanism of mudflows and other mass movements. Géotechnique 21:353–358

Ishihara K (1993) Liquefaction and flow failure during earthquakes. Géotechnique 43(3):351–415

Iverson RM (1997) The physics of debris flow. Rev Geophys 35:245–296

Iverson RM, LaHussen RG (1989) Dynamic pore-pressure fluctuations in rapidly shearing granular materials. Science 246:796–799

Kagawa T (1978) On the similitude in model vibration tests of earth-structures. Proc Jpn Soc Civil Eng 275:69–77 (in Japanese with English abstract)

Kiyama H, Fujimura H (1983) Application of Cundall's discrete block method to gravity flow analysis of rock-like granular materials. Proc Jpn Soc Civil Eng 333:137–146 (in Japanese with English abstract)

Kiyama H, Nishimura T, Fujimura H (1994) An advanced distinct element model coupling with pore water. Proc Jpn Soc Civil Eng 499:31–39 (in Japanese with English abstract)

Mizuyama T (1979) Estimation of impulsive forces of debris flows to check dams and its problems. Shin Sabo (J Soil Eros Control Eng) 32(1):40–43 (in Japanese)

Ng TT, Dobry R (1994) Numerical simulations of monotonic and cyclic loading of granular soils. ASCE J Geotech Eng Div 120:388–403

Ohmachi T, Arai Y (1986) How to determine mechanical properties for distinct element method. J Struct Eng 32A:715–723 (in Japanese with English Abstract)

Okada Y (2011) Shear behaviour in numerical triaxial compression tests by 3D fluid-coupled DEM: a fundamental study on mechanisms of landslide initiation. J For Res 16:116–127

Okada Y, Ochiai H (2007) Coupling pore-water pressure with distinct element method and steady state strengths in numerical triaxial compression tests under undrained conditions. Landslides 4:357–369

Okada Y, Ochiai H (2008) Flow characteristics of 2-phase granular mass flows from model flume tests. Eng Geol 97:1–14

Okura Y, Kitahara H, Sammori T, Kawanami A (2000) The effects of rockfall volume on runout distance. Eng Geol 58:109–124

Poulos SJ (1981) The steady state deformation. ASCE J Geotech Eng Div 107(GT5):553–562

Sassa K (1996) Prediction of earthquake induced landslides, Special Lecture of 7th International Symposium on Landslides, "Landslides," Trondheim, Norway, pp 115–132

Scheidegger AE (1973) On the prediction of the reach and velocity of catastrophic landslides. Rock Mech 5:231–236

Seed HB (1979) Soil liquefaction and cyclic mobility evaluation for level ground during earthquakes. ASCE J Geotech Eng Div 105:201–255

Shreve RL (1966) Sherman landslide, Alaska. Science 154: 1639–1643

Shreve RL (1968) Leakage and fluidization in air-layer lubricated avalanches. Geol Soc Am Bull 79:653–658

Tarumi Y, Hakuno M (1987) A granular assembly simulation for the liquefaction of sand and quicksand. In: Bulletin of Earthquake Research Institute, University of Tokyo, vol 62, pp 535–577 (in Japanese with English abstract)

Uchida Y, Hakuno M (1988) Analysis of dry rock avalanches and debris flows by granular assembly simulation. In: Bulletin of Earthquake Research Institute, University of Tokyo, vol 65, pp 321–411